RSC Advances

PAPER

View Article Online
View Journal | View Issue

Cite this: *RSC Adv.*, 2014, **4**, 7805

Electrophoretic deposition of TiO_2 nanorods for low-temperature dye-sensitized solar cells

Fang Shao, Jing Sun,* Lian Gao, Jiazang Chen and Songwang Yang

Received 4th December 2013
Accepted 9th January 2014

DOI: 10.1039/c3ra47286h

www.rsc.org/advances

The fabrication of low-temperature photoanodes is essential for flexible dye-sensitized solar cells. Electrophoretic deposition (EPD) represents a potential alternative to form photoanodes at low temperature. To optimize the photoanodes fabricated by EPD, TiO_2 nanorod/nanoparticle (labeled as NRP) structures were synthesized. The obtained NRPs have high surface charges and wide size distribution, making them suitable to form binder-free photoanodes with EPD. Compared with reference DSSCs produced with P25 (commercial TiO_2 particles), NRP based DSSCs showed enhanced light-scattering property and decreased recombination. Further, under the same total time, the efficiencies of the devices obtained with multiple EPD are above 2.2 times those of one step devices. Without any calcination or compression, the best device (with multiple EPD and a thin layer of nanoparticles) gives a conversion efficiency of 4.35%, having a short circuit current density, open circuit voltage, and filling factor of 8.41 mA cm^{-2}, 0.74 V and 69.75%, respectively.

1. Introduction

As promising devices for low-cost and environmental friendly solar energy conversion, dye-sensitized solar cells (DSSCs) have attracted much attention since Grätzel made a great breakthrough in 1991.[1–5] The photoanode typically consisting of mesoporous TiO_2 on a substrate is one of the most important components. The conventional method to connect TiO_2 nanoparticles to a substrate is paste-coating (PC), which needs high temperature calcination (450–550 °C) to remove the organic additive. Obviously, the process restricts the development of plastic-based DSSCs and raises the production costs.

Electrophoretic deposition (EPD) represents a potential alternative to form photoanodes at low temperature.[6–9] In a typical EPD process, the particles suspended in a solvent migrate under the electric field, depositing onto a substrate and thereby forming uniform films. When conducting EPD, particles to be deposited should have electrical charges not only to overcome the gravity and friction force but also to form film in an electrical field.[10] The EPD syntheses have several advantages including low cost, simple apparatus, short deposition time, green (uses no binder) and controllable film thickness.[11–14] In addition, EPD has few or no restrictions for the shape and size of the substrate.[15,16] Hsisheng Teng *et al.*[17] reported that the transport time of electron in EPD films was much shorter than in PC films. DSSCs assembled with EPD films outperformed those devices with PC films by 15% in solar energy conversion efficiency. Besides commercial nanoparticles, mesoporous TiO_2 nanoparticle (*ca.* 260 nm) films were also prepared through an EPD process to reduce the grain boundaries and improve the light scattering.[18]

It has been demonstrated that nanorod can facilitate electron transport by decreasing grain boundaries and increase the electron lifetime *via* suppressing charge recombinations.[19–21] However, due to the lack of surface charges, TiO_2 nanorods were difficult to deposit on substrates without surfactant. Therefore, little information is available on the DSSCs based on EPD TiO_2 nanorods with no use of additives.

Here, we synthesized TiO_2 nanorods (NR) *via* a hydrothermal method and increase their surface charges effectively by $TiCl_4$ solution treatment. The treated samples were TiO_2 nanorod/nanoparticle structures (labeled as NRP). NRP was easy to deposit on FTO glass with a low current EPD process. The performances of the NRP-DSSCs were compared with reference DSSCs produced by EPD technique with NR particles and commercial P25-TiO_2 particles. A multiple EPD process was adopted to avoid cracks and also to enhance the connection between the nanorods. In addition, a thin layer of P25 nanoparticles was deposited on the substrate to further improve the DSSC's efficiency.

2. Experimental

2.1. Synthesis of the anatase TiO_2 nanorods

The anatase TiO_2 nanorods were synthesized by two-step hydrothermal reactions.[22–24] TiO_2 source used for producing the nanorods was P25 (Degussa AG, Germany), a commercially

The State Key Lab of High Performance Ceramics and Superfine Microstructure, Shanghai Institute of Ceramics, Chinese Academy of Sciences, 1295 Ding Xi Road, Shanghai 200050, China. E-mail: jingsun@mail.sic.ac.cn; Fax: +86 21 52413903; Tel: +86 21 52414301

available TiO_2 powder, which consists of about 30% rutile and 70% anatase with a primary particle size of about 20 nm. In a typical procedure, 2 g P25 was added into 40 mL 10 M NaOH aqueous solution. Then the mixture was subjected to a hydrothermal treatment at 130 °C for 20 h. The resulting slurries were filtered and washed with 0.1 M HNO_3 to adjust the pH to 5.4. After that, the suspensions were transferred to an autoclave and kept in an electric oven at 175 °C for 48 h. After being calcined at 450 °C for 30 min, nanorods labeled as NR were obtained. NR was treated with 0.2 M $TiCl_4$ at 60 °C for 1 h and then annealed at 450 °C for 30 min. The obtained samples were denoted as NRP.

2.2. Electrodeposition of TiO_2

The deposition was performed on FTO (F–SnO_2 coated glass) substrates using an electrophoretic deposition technique. The EPD bath consists of a FTO cathode, a FTO anode and TiO_2 suspension. Isopropanol were employed as a media and the concentration of TiO_2 was either 3 g L^{-1} or 6 g L^{-1}. After 30 min of ultrasonication, the suspensions were ready to use. The distance between the two electrodes was fixed at 1 cm and the constant current mode (−10 μA) was applied with a Keithley 2400 Source Meter. Then, the coated samples were dried under ambient condition to get photoanodes.

2.3. Solar cell fabrication

After being heated at 100 °C for 30 min, the as-prepared photoanodes were immersed into a 0.3 mM N719 dye solution in a mixed solvent of 1 : 1 acetonitrile/*tert*-butyl alcohol at room temperature for 24 h. These sensitized photoanodes and the Pt–FTO counter electrodes were assembled as sandwich-type cells which separated by polymer foils. The space between the two electrodes was filled with liquid electrolyte. The electrolyte composition was 0.5 M LiI, 0.05 M I_2 and 0.5 M *tert*-butylpyridine in acetonitrile.

2.4. Characterization

Structural characterization of the synthesized films was done using a powder X-ray diffraction (XRD, D/max 2550 V, Rigaku Tokyo, Japan). The morphology was obtained by field emission scanning electron microscopy (FESEM, JSM-6700F, JEOL Tokyo, Japan) and the details of the structure were determined with transmission electron microscopy (TEM/HRTEM, JEM-200CX, JEOL Tokyo, Japan), along with selected area electron diffraction (SAED) pattern. Zeta potential of NR and NRP in isopropanol was measured using a Zeta plus analyzer. The total reflection of the samples were recorded with a lambda-950 UV-Vis spectrophotometer (Perkin Elmer, Waltham, MA). *J–V* curves were recorded by a Keithley Series 2400 System Source Meter Instrument. The irradiation source is a solar simulator (Newport) giving AM 1.5 G illumination on the surface of the solar cells. The active area of photoanodes was 0.12 cm^2 determined by an aperture mask. Dark current voltage characteristics were performed on CHI 660D electrochemical workstation. Electrochemical impedance spectroscopy (EIS) curves of the DSSCs were also observed. The frequency range was varied from 0.1 Hz to 100 kHz. The applied bias voltage was set to the open-circuit voltage (V_{OC}) of the DSSC, which had been determined earlier.

3. Results and discussion

As shown in Fig. 1, P25 consists of rutile and anatase while NR is of pure anatase. Sharp diffraction peaks imply that the as-prepared NR has excellent crystallinity. After $TiCl_4$ treatment, there was a weak peak of rutile at 27.5°.

Fig. 2 shows the photographs of NR and NRP suspensions. The two samples were ultrasonically dispersed for 30 min and then placed for 4 h and overnight to see the dispersancy. It can be perceived that the NRP can be stably dispersed in isopropanol. On the contrary, NR was easy to precipitate, this may be due to the lack of sufficient charges on nanorods.[25] In order to convince this, Zeta potentials of the suspended NR and NRP in isopropanol were measured and the values were +6.56 mV and +18.6 mV, respectively. The both two samples have positive zeta potentials when suspended in isopropanol. However, the zeta potential value of NRP was approximately three times that of NR, suggesting that the two samples have different surface chemical properties.[11] This is coincident with the good dispersion of NRP shown in Fig. 2.

Fig. 3a and b are SEM images of NR and NRP powders. For NR, the distinct rod morphology with smooth and clean surfaces can be observed. Both large and small nanorods, and even nanoflakes can be observed in the sample. The diameters of the nanorods are 15–100 nm and the lengths ranged from 30 nm to 500 nm. The nanorods with wide size distribution can take advantage of both high surface area and high light utilization.[26] After $TiCl_4$ treatment, the nanorod morphology sustained while the surfaces became rough.

Further analyses of NRP with TEM are depicted in Fig. 3c and d. It can be observed that a thin layer had covered nanorods homogeneously. Based on HRTEM and SAED images (Fig. 3d), the nanorod can be indexed to single-crystalline anatase with [001] as the growth direction. The extra diffraction spots in

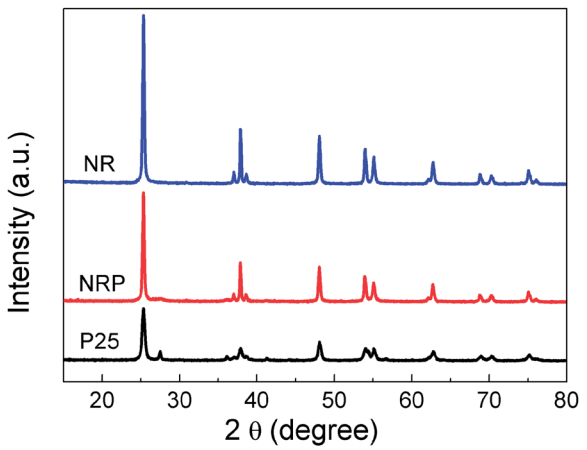

Fig. 1 XRD patterns of P25, NR and NRP powders.

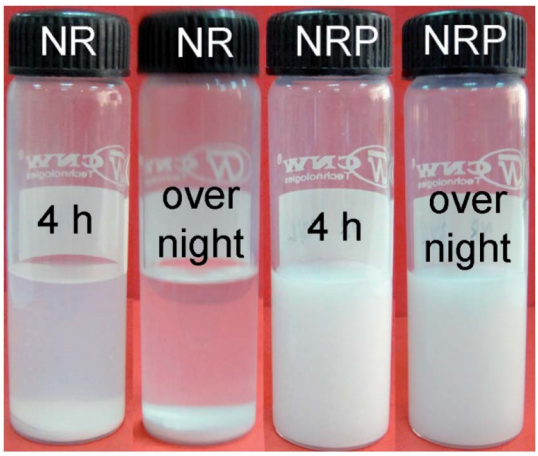

Fig. 2 Digital photographs of NR and NRP suspensions after standing for 4 h and overnight.

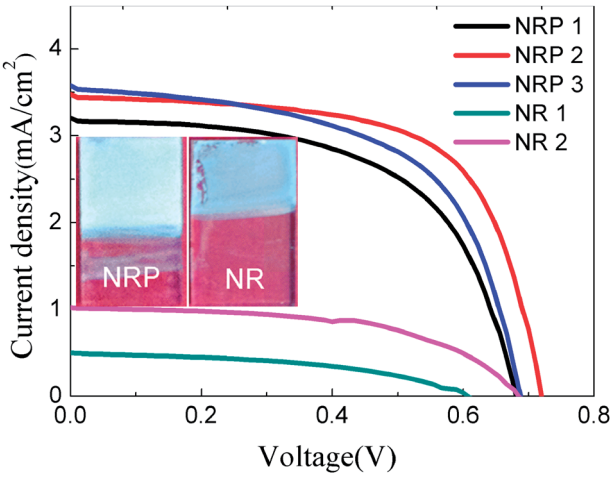

Fig. 4 J–V characteristics of DSSCs assembled with NRP and NR photoanodes (TiO_2 concentration: 3 g L^{-1}).

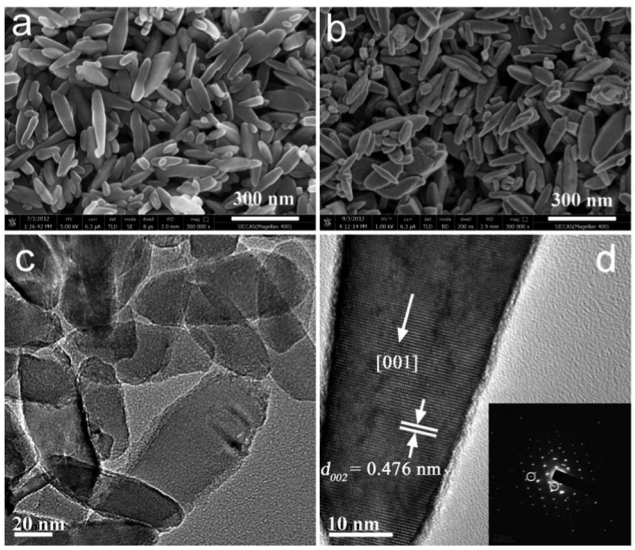

Fig. 3 (a) SEM image of NR powders, (b) SEM image of NRP powders, (c) low-magnification TEM image of NRP powders, (d) HRTEM image of a single NRP nanoparticle, inset: the corresponding SAED pattern.

SAED pattern (marked by white circles) may result from the coating layer or the adjacent grain.

When being used in an EPD process, the solid to liquid ratio of the suspension fluid used for EPD was determined to as low as 3 g L^{-1} to avoid the fast precipitation of NR powders. Without any surfactant, NR could hardly be deposit on FTO glasses. As demonstrated above, the difficulty was ascribed to low amount of surface charge on NR. Photographs of NR and NRP films with the same deposition time (40 min) are shown in Fig. 4. It is obvious that NR film is much thinner than NRP film. The NR and NRP films with different deposition times were consequently examined as photoanodes in DSSCs after sensitized with dye N719. Fig. 4 shows the corresponding photovoltaic curves under illumination of simulated AM 1.5 G solar light (100 mW cm^{-2}). All of the detailed values and preparation conditions and are shown in Table 1. For NR-DSSCs, the efficiencies are less than 0.5% due to their very thin TiO_2 films. In the case of DSSC with NRP1, the short-circuit current density (J_{SC}), open-circuit photovoltage (V_{OC}) and fill factor (FF) values are 3.18 mA cm^{-2}, 0.68 V, and 58.43%, respectively, with an overall power conversion efficiency (η) of 1.26%. When the deposition time increased to 20 min, the efficiency increased to 1.60%. With thicker films, NRP3 electrode showed higher J_{sc}. However, the values of V_{OC} and FF decreased, leading to a lower efficiency. The thickness increased from 5.58 μm to only 7.25 μm when the EPD time rose from 20 min to 40 min. This may attribute to the low amount of content of NRP particles. TiO_2 concentration was increased in order to further enhance the photoanodes' thickness and the dye absorption.

When the NRP concentration is 6 g L^{-1}, the measured J–V curves of the corresponding DSSCs are shown in Fig. 5. The photovoltaic performances and the thickness of the photoanodes were summarized in Table 2. The NRP-20 and NRP2 electrodes have very approximate thickness and efficiency values. However, compared with NRP3, the thickness of NRP-40 is enhanced (nearly twice than that of NRP-20). It indicates that there are sufficient particles until deposited for 40 min.

In addition, a multiple EPD process was adopted to further improve the performance. The multiple EPD process can be divided into a few 5 min deposition steps. In a typical 5 min

Table 1 Preparation conditions and performance characteristics of DSSCs based on NRP and NR photoanodes (TiO_2 concentration: 3 g L^{-1})

Photoanodes	Time (min)	Thickness (μm)	V_{OC} (V)	J_{SC} (mA cm^{-2})	FF (%)	η (%)
NRP1	10	3.73	0.68	3.18	58.43	1.26
NRP2	20	5.58	0.72	3.45	64.45	1.60
NRP3	40	7.25	0.69	3.54	58.31	1.42
NR1	20	0.58	0.61	0.50	45.89	0.14
NR2	40	0.94	0.68	1.02	55.53	0.39

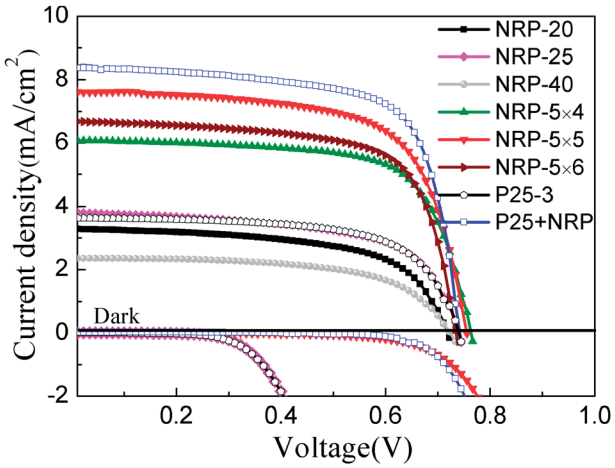

Fig. 5 *J–V* characteristics of DSSCs assembled with different TiO_2 photoanodes (TiO_2 concentration: 6 g L^{-1}).

Table 2 Preparation conditions and performance characteristics of DSSCs based on various photoanodes (TiO_2 concentration: 6 g L^{-1})

Photoanodes	Time (min)	Thickness (μm)	V_{OC} (V)	J_{SC} (mA cm^{-2})	FF (%)	η (%)
NRP-20	20	5.28	0.72	3.28	60.32	1.42
NRP-25	25	6.15	0.74	3.81	61.09	1.72
NRP-40	40	9.73	0.72	2.35	60.70	1.03
NRP-5 × 4	5 × 4	4.32	0.76	6.09	68.67	3.20
NRP-5 × 5	5 × 5	4.87	0.76	7.61	66.61	3.83
NRP-5 × 6	5 × 6	5.70	0.73	6.68	68.55	3.36
P25-3	3	6.33	0.74	3.64	64.58	1.74
P25 + NRP	0.3 + 5 × 5	4.96	0.74	8.41	69.75	4.35

step, the samples were deposited for 5 min and then dried in air. This step was then repeated three times to get NRP-5 × 4. Similarly, there were five and six 5 min-steps in preparing NRP-5 × 5 and NRP-5 × 6 respectively. Although we maintained the same total time in sample NRP-20, NRP-5 × 4 (20 min) and NRP-25, NRP-5 × 5 (25 min), the results exhibit quite large difference in film thickness. Each time, some particles are filled in the cracks or pores produced in the previous EPD process, therefore the films obtained by multiple depositions are much thinner.[27] Multiple electrophoretic depositions can improve the DSSCs efficiency remarkably. Comparing NRP-20 cell with NRP-5 × 4 cell, an 86% increase in the J_{SC} and a 14% increase in the FF was obtained, leading to a 125% increase in the conversion efficiency. Similarly, NRP-5 × 5 gives a great improvement of J_{SC}, a superior FF and V_{OC}, thus the efficiency of NRP-5 × 5 were about double that of NRP-25. The improved FF might be due to the improved electrical contact at the FTO/TiO_2 interface.[28] To further improve the performance, a thin layer of P25 particles was first electrophoretic deposited on FTO glass for 18 s. After dried, NRP was then deposited with five 5 minute steps (5 × 5). The obtained P25 + NRP device has the best photovoltaic performance. Its short circuit current density (J_{SC}), open circuit voltage (V_{OC}), and filling factor (FF) are 8.41 mA cm^{-2}, 0.74 V, and 69.75%, respectively, yielding an overall conversion efficiency of 4.35%.

Fig. 5 also shows the dark current of NRP-25, NRP-5 × 5, P25-3 and P25 + NRP cells. The dark current is correlated to the recombination of electrons with redox mediator in the electrolyte.[29] The onset of the dark current of NRP-25 and P25-3 occurred at lower forward bias. A multiple method can suppress the dark current, shifting the onset by several hundred millivolts. The low recombination reaction can increase the electron density of the TiO_2 film, leading to an enhancement in the resulting V_{OC}.[28,30] As a result, the decrease of dark current can provoke the increase of open-circuit photovoltage.

The structures of the NRP-25, NRP-5 × 5 and P25 + NRP photoanodes were characterized with SEM as shown in Fig. 6. The images exhibit that NRP form porous structures. There are microcracks in the one-step process deposited films (Fig. 6a) while NRP-5 × 5 films are free of cracks (Fig. 6b). For P25 + NRP film, the P25 layer is about 600 nm thick. In addition, nanoflakes and nanorods are present in the P25 layer (marked by white circles in Fig. 6d). These results suggest that the multiple EPD could fill the cracks and pores produced in the last EPD to form a better quality microstructure photoanode.

The scattering characters of various photoanodes were also investigated through reflectance spectra (Fig. 7). It is apparent that the four reflection curves have a highly similar profile and the intensity of NRP samples are all enhanced compared with that of P25, pointing out the good scattering property of NRP. When the size of the particles is comparable to the wavelength of the incident light, light can be scattered and redirected in various directions, leading to the enhancing of the light-harvesting efficiency. Besides, the reflection under 400 nm decreases dramatically due to the light absorption caused by the band transition of TiO_2.[31]

In order to understand the electron transport and recombination properties in various DSSCs, we further measured the electrochemical impedance spectroscopy (EIS) in the frequency range of 0.1 Hz–100 kHz. Nyquist plots with four kinds of EPD electrodes at forward bias of the open-circuit voltage were shown in Fig. 8. Generally, three characteristic semicircles can

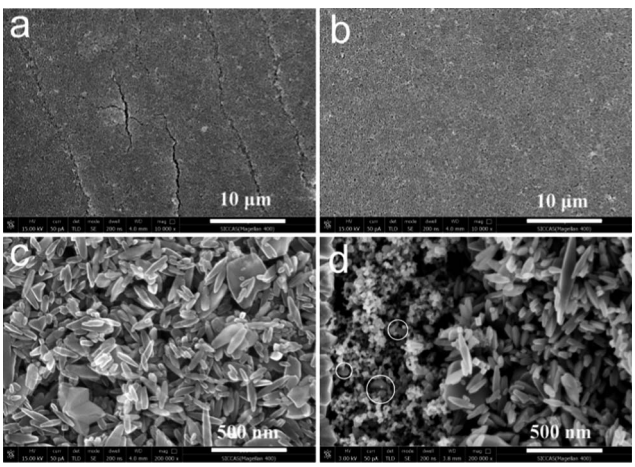

Fig. 6 Plane SEM images of (a) NRP-25 photoanode, (b) NRP-5 × 5 photoanode, (c) NRP-5 × 5 photoanode at higher magnifications, (d) cross-sectional SEM images of P25 + NRP photoanode.

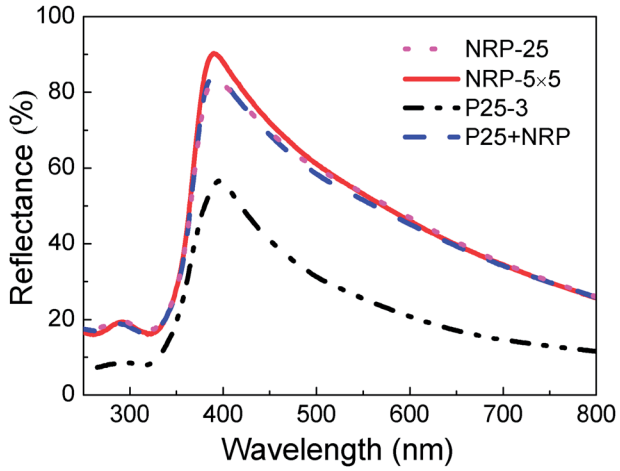

Fig. 7 Reflectance spectra of four different photoanodes.

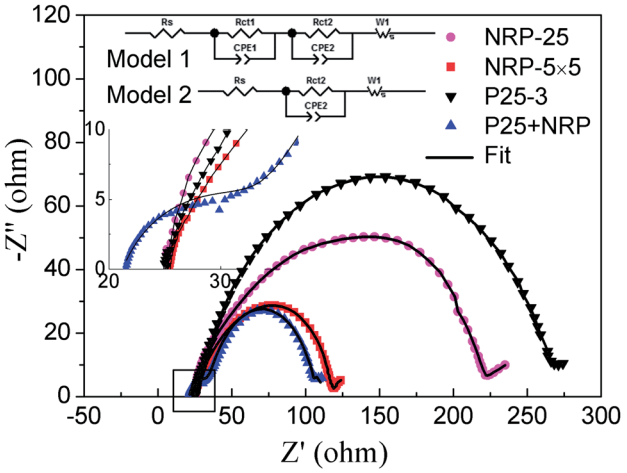

Fig. 8 Electrochemical impedance spectra of the TiO_2 nanostructures. Inset: the enlarged high frequency image taken from the areas marked with the black square.

be obtained from EIS spectra.[32–34] The small semicircle occurring at high frequency (in the kHz range) is related to the charge transfer at the platinum counter electrode/electrolyte interface. The large one at the lower frequency (in the 10–100 Hz range) is attributed to electron charge transfer resistance at the TiO_2/dye/electrolyte interface (Rct2), dominating the impedance of the DSSCs. The small feature (in the mHz range) is attributed mainly to the Nernst diffusion of I_3^- within the electrolyte. As shown in the inset image of Fig. 8, the high frequency semicircles at in sample NRP-25, NRP-5 × 5 and P25-3 are all overlapped together, showing semicircles in the middle frequency. This is probably due to the poor connection between the TiO_2 particles and the substrate.[35] With a thin layer of P25, the high frequency semicircle is presented, pointing out the superior connection. The semicircle size in middle-frequency decreases in the order of P25-3, NRP-25, NRP-5 × 5 and P25 + NRP, owing to the gradually acceleration of electron transfer process in the photoanode.[36] Furthermore, the charge transfer resistance of the DSSCs was analyzed by Z-view software. According to the EIS model reported in the literature,[20,27,37,38] two equivalent circuits containing constant phase elements (CPE) and resistances (R) were adopt for P25 + NRP (Model 1) and three other samples (Model 2). The fitting values of Rct2 for NRP-25, NRP-5 × 5, P25-3 and P25 + NRP electrodes are 204.7, 96.9, 245.2 and 72.3 Ω, respectively. It confirms that the Rct2 decreases dramatically with multiple depositions, especially by introducing a thin layer of P25. The decrease of Rct2 can enhance the photogenerated electron collection from TiO_2 surface to FTO substrate, resulting in an increase of J_{SC}.[35,39] This is highly consistent with the measured results.

4. Conclusion

In this work, TiO_2 nanorods with high surface charges (NRP) was successfully synthesized using TiO_2 nanorods (NR) as precursor. The NRP showed fewer grain boundaries, defects and higher light scattering with reference to corresponding properties of commercial P25–TiO_2 particles. Without any additive, NRP-photoanodes can be prepared with a low current electrophoretic deposition (EPD) process under room temperature. In addition, a multiple EPD process was adopted to form a better quality microstructure photoanode. Under the same total time, the efficiencies of the multiple devices are above 2.2 times those of one-step devices. To further improve the performance, a thin layer of P25 particles was electrophoretic deposited on FTO glass for 18 s. The P25 + NRP device has the best photovoltaic performance. Its short circuit current density (J_{SC}), open circuit voltage (V_{OC}), and filling factor (FF) are 8.41 mA cm^{-2}, 0.74 V, and 69.75%, respectively, yielding an overall conversion efficiency of 4.35%.

Acknowledgements

This work was supported by the National Natural Science Foundation of China (Grant no. 50972157, 51072215).

References

1 B. Oregan and M. Grätzel, *Nature*, 1991, **353**, 737–740.
2 H. Lindstrom, A. Holmberg, E. Magnusson, S. E. Lindquist, L. Malmqvist and A. Hagfeldt, *Nano Lett.*, 2001, **1**, 97–100.
3 D. Kim, K. Lee, P. Roy, B. I. Birajdar, E. Spiecker and P. Schmuki, *Angew. Chem., Int. Ed.*, 2009, **48**, 9326–9329.
4 Q. F. Zhang, T. R. Chou, B. Russo, S. A. Jenekhe and G. Z. Cao, *Angew. Chem., Int. Ed.*, 2008, **47**, 2402–2406.
5 Q. F. Zhang and G. Z. Cao, *Nano Today*, 2011, **6**, 91–109.
6 Z. S. Xue, W. Zhang, X. Yin, Y. M. Cheng, L. Wang and B. Liu, *RSC Adv.*, 2012, **2**, 7074–7080.
7 H. W. Chen, C. Y. Lin, Y. H. Lai, J. G. Chen, C. C. Wang, C. W. Hu, C. Y. Hsu, R. Vittal and K. C. Ho, *J. Power Sources*, 2011, **196**, 4859–4864.
8 T. Miyasaka and Y. Kijitori, *J. Electrochem. Soc.*, 2004, **151**, A1767–A1773.
9 A. Chavez-Valdez and A. R. Boccaccini, *Electrochim. Acta*, 2012, **65**, 70–89.

10 Z. S. Xue, L. Wang and B. Liu, *Nanoscale*, 2013, **5**, 2269–2273.
11 Y. Hara, J. R. S. Brownson and M. A. Anderson, *Int. J. Appl. Ceram. Technol.*, 2012, **9**, 115–123.
12 F. Hosseinbabaei and B. Raissidehkordi, *J. Eur. Ceram. Soc.*, 2000, **20**, 2165–2168.
13 J. Chen, W. Lei, C. Li, Y. Zhang, Y. P. Cui, B. P. Wang and W. Q. Deng, *Phys. Chem. Chem. Phys.*, 2011, **13**, 13182–13184.
14 A. Salant, M. Shalom, I. Hod, A. Faust, A. Zaban and U. Banin, *ACS Nano*, 2010, **4**, 5962–5968.
15 C. Y. Lin, Y. H. Lai, H. W. Chen, J. G. Chen, C. W. Kung, R. Vittal and K. C. Ho, *Energy Environ. Sci.*, 2011, **4**, 3448–3455.
16 W. W. Tan, X. Yin, X. M. Zhou, J. B. Zhang, X. R. Xiao and Y. Lin, *Electrochim. Acta*, 2009, **54**, 4467–4472.
17 Y. J. Liou, P. T. Hsiao, L. C. Chen, Y. Y. Chu and H. S. Teng, *J. Phys. Chem. C*, 2011, **115**, 25580–25589.
18 H. W. Chen, C. P. Liang, H. S. Huang, J. G. Chen, R. Vittal, C. Y. Lin, K. C. Wu and K. C. Ho, *Chem. Commun.*, 2011, **47**, 8346–8348.
19 S. H. Kang, S. H. Choi, M. S. Kang, J. Y. Kim, H. S. Kim, T. Hyeon and Y. E. Sung, *Adv. Mater.*, 2008, **20**, 54–58.
20 J. Q. Luo, L. Gao, J. Sun and Y. Q. Liu, *RSC Adv.*, 2012, **2**, 1884–1889.
21 M. Law, L. E. Greene, J. C. Johnson, R. Saykally and P. D. Yang, *Nat. Mater.*, 2005, **4**, 455–459.
22 T. Y. Tsai and S. Y. Lu, *Electrochem. Commun.*, 2009, **11**, 2180–2183.
23 Y. X. Yu and D. S. Xu, *Appl. Catal., B*, 2007, **73**, 166–171.
24 J. N. Nian and H. S. Teng, *J. Phys. Chem. B*, 2006, **110**, 4193–4198.
25 A. C. Zaman, C. B. Ustundag, F. Kaya and C. Kaya, *Mater. Lett.*, 2012, **66**, 179–181.
26 Z. S. Wang, H. Kawauchi, T. Kashima and H. Arakawa, *Coord. Chem. Rev.*, 2004, **248**, 1381–1389.
27 W. H. Chiu, K. M. Lee and W. F. Hsieh, *J. Power Sources*, 2011, **196**, 3683–3687.
28 J. Xia, N. Masaki, K. Jiang and S. Yanagida, *J. Phys. Chem. B*, 2006, **110**, 25222–25228.
29 S. Ito, P. Liska, P. Comte, R. L. Charvet, P. Pechy, U. Bach, L. Schmidt-Mende, S. M. Zakeeruddin, A. Kay, M. K. Nazeeruddin and M. Grätzel, *Chem. Commun.*, 2005, 4351–4353.
30 Z. P. Zhang, S. M. Zakeeruddin, B. C. O'Regan, R. Humphry-Baker and M. Grätzel, *J. Phys. Chem. B*, 2005, **109**, 21818–21824.
31 Z. P. Tian, H. M. Tian, X. Y. Wang, S. K. Yuan, J. Y. Zhang, X. B. Zhang, T. Yu and Z. G. Zou, *Appl. Phys. Lett.*, 2009, 94.
32 Z. S. Yang, C. Y. Chen, C. W. Liu, C. L. Li and H. T. Chang, *Adv. Energy Mater.*, 2011, **1**, 259–264.
33 Q. Wang, J. E. Moser and M. Grätzel, *J. Phys. Chem. B*, 2005, **109**, 14945–14953.
34 X. J. Lu, X. L. Mou, J. J. Wu, D. W. Zhang, L. L. Zhang, F. Q. Huang, F. F. Xu and S. M. Huang, *Adv. Funct. Mater.*, 2010, **20**, 509–515.
35 X. Yin, Z. S. Xue, L. Wang, Y. M. Cheng and B. Liu, *ACS Appl. Mater. Interfaces*, 2012, **4**, 1709–1715.
36 S. R. Sun, L. Gao and Y. Q. Liu, *Appl. Phys. Lett.*, 2010, **96**, 083113.
37 N. L. Yang, J. Zhai, D. Wang, Y. S. Chen and L. Jiang, *ACS Nano*, 2010, **4**, 887–894.
38 Z. R. Wang, H. Wang, B. Liu, W. Z. Qiu, J. Zhang, S. H. Ran, H. T. Huang, J. Xu, H. W. Han, D. Chen and G. Z. Shen, *ACS Nano*, 2011, **5**, 8412–8419.
39 S. Ito, N. L. C. Ha, G. Rothenberger, P. Liska, P. Comte, S. M. Zakeeruddin, P. Pechy, M. K. Nazeeruddin and M. Grätzel, *Chem. Commun.*, 2006, 4004–4006.

